

THE DENSITY GRADIENT INSIDE MOLECULAR-GAS CLUMPS AS A BOOSTER OF THEIR STAR FORMATION ACTIVITY

G. PARMENTIER¹

Accepted for publication in ApJ

ABSTRACT

Star-forming regions presenting a density gradient experience a higher star formation rate than if they were of uniform density. We refer to the ratio between the star formation rate of a spherical centrally-concentrated gas clump and the star formation rate that this clump would experience if it were of uniform density as the magnification factor ζ . We map ζ as a function of clump mass, radius, initial volume density profile and star formation time-span. For clumps with a steep density profile (i.e. power-law slope ranging from -3 to -4 , as observed in some high-density regions of Galactic molecular clouds), we find the star formation rate to be at least an order of magnitude higher than its top-hat equivalent. This implies that such clumps experience faster and more efficient star formation than expected based on their mean free-fall time. This also implies that measurements of the star formation efficiency per free-fall time of clumps based on their global properties, namely, mass, mean volume density and star formation rate, present wide fluctuations. These reflect the diversity in the density profile of star-forming clumps, not necessarily variations in the physics of star formation. Steep density profiles inside star-cluster progenitors may be instrumental in the formation of multiple stellar populations, such as those routinely observed in old globular clusters.

Subject headings: galaxies: star clusters: general — stars: formation — ISM: clouds

1. INTRODUCTION

The process of star formation is the engine of galaxy evolution. Galaxies form a significant fraction of their stars inside clumps of dense molecular gas, themselves embedded in more diffuse giant molecular clouds, with respective spatial scales of 1 parsec and a few tens of parsecs. Distant galaxies, molecular clumps of the Galactic disk and molecular clouds of the Solar neighbourhood present a linear correlation between their dense-gas mass and star formation rate (Gao & Solomon 2004; Wu et al. 2010; Lada, Lombardi & Alves 2010). It thus seems that the activity of a star-forming region is controlled by its dense-gas content, usually defined as gas with a number density higher than $\sim 10^4 \text{ cm}^{-3}$, equivalent to a mass density of $700 M_{\odot} \cdot \text{pc}^{-3}$. Yet, this correlation comes with a scatter. Is this scatter driven by observational uncertainties only? Or does it conceal secondary, yet to be discovered, properties? Consider for instance two star-forming regions with different star formation rates. Does the more active star-forming region necessarily contain a larger dense-gas mass? Or could its higher star formation rate result from its dense-gas clumps being more efficient at forming stars than those of the less active region, without modification of the overall dense-gas content?

While the interplay between the star formation rate of molecular clouds and the spatial distribution of their gas has been well-studied, both observationally (see e.g. Lada et al. 2013; Kainulainen et al. 2014) and theoretically (Cho & Kim 2011; Elmegreen 2011), the interplay between star formation rate and gas spatial distribution of small-scale roughly-spherical molecular clumps has received less attention. In the disk of our Galaxy, the den-

sity profile inside molecular clumps obeys a power-law $\rho(r) \propto r^{-p}$, with $\rho(r)$ the gas volume density at a distance r from the clump center and p observed to range from 1.2 to 2.5 (Müller et al. 2002). The star formation rate of clumps with $p \simeq (1.5, 2.0)$ is predicted to be 1.6-to-2 times higher than the star formation rate of clumps containing the same gas mass inside the same radius, but with a top-hat profile ($p = 0$). Assuming a pure power-law of slope -1.5 for the volume density profile of clumps, Tan et al. (2006) predict a star formation rate 1.6 times higher than if they were of uniform density (see eq. 2 in Tan et al. 2006). For a clump with a density profile of slope -2 combined to a small ($\simeq 10^{-2}$ the clump radius) central core, Parmentier (2014) finds that the star formation efficiency achieved within one free-fall time amounts to $1.6\epsilon_{\text{ff}}$, rather than ϵ_{ff} , with ϵ_{ff} the star formation efficiency per free-fall time. Additionally, Fig. 9 in Parmentier & Pfalzner (2013) shows that the star formation efficiency of a clump increases faster with time when the clump density profile is steeper. Numerical simulations confirm these analytical and semi-analytical insights. Girichidis et al. (2011) performed hydrodynamical simulations of molecular clumps with an initial gas mass of $100 M_{\odot}$, a radius of 0.1 pc, various initial gas density profiles and turbulence seeds. Their fig. 3 shows that, once star formation has started, the mass in sink particles grows faster for an initial gas density profile of slope -2 than for a top-hat density profile. Specifically, the rate at which the gas mass is accreted onto the sink particles is twice as high for the power-law density profile with a slope of -2 as it is for its top-hat equivalent. In other words, more centrally-concentrated clumps show a higher star formation rate as a result of the higher gas volume densities and shorter free-fall times characterizing their inner regions. Finally,

¹ Astronomisches Rechen-Institut, Zentrum für Astronomie der Universität Heidelberg, Mönchhofstr. 12-14, D-69120 Heidelberg, Germany

similar conclusions were reached by Elmegreen (2011) based on the gas density-PDF. Modelling the density PDF of a spherically-symmetric cloud as the convolution of the log-normal PDF from turbulence for cloud local regions (where the gas volume density does not vary significantly) with the overall cloud density profile, he too concludes that the star formation rate of centrally-concentrated clouds is higher than that of clouds of uniform density. All studies above have considered gas density profiles no steeper than $\rho(r) \propto r^{-2}$.

But recent observations have reported much steeper density profiles in dense-gas clumps of the Galactic molecular clouds MonR2 and NGC6334, with $p \simeq (3, 4)$ (Schneider et al. 2015). These unlock a different regime of star formation activity: when $p > 2$, not only do clump inner regions present a faster pace of star formation, they also contain most of the clump mass. This raises a tantalizing question: by how much do so steep density profiles increase the clump star formation rate compared to uniform-density clumps with identical mass and radius? A comprehensive mapping of this effect was still missing, as well as a method to quantify it once star formation has modified the initial gas distribution.

Not only does a gas density gradient inside clumps impact their star formation rate, it also affects the star formation efficiency per free-fall time that we measure for such clumps. The star formation efficiency per free-fall time, ϵ_{ff} , is a dimensionless key parameter related to the star formation rate of galaxies, clouds and clumps. It quantifies the gas mass fraction that a gas reservoir turns into stars every free-fall time $\langle \tau_{\text{ff}} \rangle$, with the free-fall time $\langle \tau_{\text{ff}} \rangle$ calculated at the gas mean density. A proxy to the star formation rate of a galaxy, cloud, or clump is thus, with m_{gas} its star-forming gas mass:

$$SFR = \frac{\epsilon_{\text{ff}} m_{\text{gas}}}{\langle \tau_{\text{ff}} \rangle} \quad (1)$$

(see e.g. Krumholz & McKee 2005; Krumholz & Tan 2007; Evans et al. 2009; Lada, Lombardi & Alves 2010; Murray 2011; Krumholz, Dekel & McKee 2012; Vutisalchavakul, Evans & Heyer 2016; Ochsendorf et al. 2017).

According to Eq. 1, to increase the star formation rate of a clump, one can increase either its mass or its volume density or its star formation efficiency per free-fall time. However, as was shown by Tan et al. (2006), Girichidis et al. (2011), Elmegreen (2011) and Parmentier (2014), one can also steepen its volume density profile. That should be taken into account when comparing star-forming regions based on their star formation efficiency per free-fall time. Whether ϵ_{ff} is constant or not remains debated. Krumholz & Tan (2007) argue that its value is about 0.01, constant in the Galactic disk across a wide range of volume densities, from low-density giant molecular clouds to high-density CS clumps (see their fig. 5). In contrast, Ochsendorf et al. (2017) argue that significant variations exist among molecular clouds of the Large Magellanic Cloud. According to their fig. 6, ϵ_{ff} ranges from $\simeq 1$ down to less than 10^{-3} , the most massive clouds being the least efficient ones (see also Murray 2011).

This debate regarding the variations of the star formation efficiency per free-fall time or the absence thereof

will not move forward unless it takes into account the impact that the structure of star-forming regions has on their star formation activity. Not only does the star formation rate depend on the star formation efficiency per free-fall time, on the mass and free-fall time of the star-forming gas, it also depends on how centrally-concentrated the gas is, an aspect which remains unaccounted for by Eq. 1.

In this contribution, we expand the cluster-formation model of Parmentier & Pfalzner (2013) to estimate the ratio between the star formation rate of centrally-concentrated clumps and the star formation rate that they would have if they were of uniform density. We refer to this ratio as the *magnification factor*, this one encapsulating the impact of the structure of a clump on its star formation rate. We also obtain the star formation efficiency per free-fall time of clumps that one would measure based on their global properties (star formation rate, gas mass and free-fall time), that is, using Eq. 1 and ignoring their degree of concentration. We are then able to contrast this *measured* star formation efficiency per free-fall time with its counterpart for a clump region small enough to be considered of uniform density, which we refer to as the *intrinsic* star formation efficiency per free-fall time (that is, by comparing the intrinsic and measured star formation efficiencies per free-fall time, we compare a local quantity with a global one). This will yield a map of how distinct *intrinsic* and *measured* star formation efficiencies per free-fall time are, as a function of other clump properties.

In the simulations presented here, the intrinsic star formation efficiency per free-fall time is assumed to be constant, both in space and in time. Our model star-forming regions are spherically-symmetric with radii ranging from a fraction of a parsec up to $\simeq 10$ pc. We coin them "clumps", while stressing that other authors may use the term "cloud" in similar contexts.

The outline of the paper is as follows. Section 2 introduces the concepts of intrinsic and measured star formation efficiencies per free-fall time, and the concept of magnification factor. Section 3 presents observational evidence from nearby molecular clouds and Sec. 4 presents the model. Section 5 maps the magnification factor as a function of clump mass, radius, density profile and time. In Sec. 6, we briefly discuss two model consequences. Conclusions are presented in Sec. 7.

2. MEASURED VS. INTRINSIC STAR FORMATION EFFICIENCY PER FREE-FALL TIME

Applying Eq. 1 to a molecular clump with known estimates of its gas mass, m_{gas} , free-fall time, $\langle \tau_{\text{ff}} \rangle$, and star formation rate, SFR_{clump} , one can derive a star formation efficiency per free-fall time:

$$\epsilon_{\text{ff, meas}} = \frac{SFR_{\text{clump}} \langle \tau_{\text{ff}} \rangle}{m_{\text{gas}}}, \quad (2)$$

which we refer to as the *measured* star formation efficiency per free-fall time. In Eq. 2, the free-fall time $\langle \tau_{\text{ff}} \rangle$ is calculated at the mean volume density $\langle \rho_{\text{gas}} \rangle$ of the clump gas:

$$\langle \tau_{\text{ff}} \rangle = \sqrt{\frac{3\pi}{32G\langle \rho_{\text{gas}} \rangle}}, \quad (3)$$

and $\epsilon_{\text{ff, meas}}$ is therefore a global value.

Although Eq. 2 does not explicitly account for the structure of the clump, it is nevertheless affected by it. To reveal this effect, we compute the total star formation rate of the clump by integrating the star formation rate of spherical shells of gas, from clump center to clump edge:

$$\begin{aligned} SFR_{clump} &= \int_0^{r_{clump}} \epsilon_{\text{ff, int}} \frac{dm_{gas}(r)}{\tau_{\text{ff}}(r)} \\ &= \int_0^{r_{clump}} \epsilon_{\text{ff, int}} \frac{4\pi r^2 \rho_{gas}(r)}{\tau_{\text{ff}}(r)} dr. \end{aligned} \quad (4)$$

Here, r_{clump} is the clump radius, $dm_{gas}(r) = 4\pi r^2 \rho_{gas}(r) dr$ is the gas mass of a spherical shell of radius r , thickness dr , gas volume density $\rho_{gas}(r)$ and free-fall time $\tau_{\text{ff}}(r)$, with $0 \leq r \leq r_{clump}$. In contrast to Eq. 3, $\tau_{\text{ff}}(r)$ is a locally-defined free-fall time, i.e.:

$$\tau_{\text{ff}}(r) = \sqrt{\frac{3\pi}{32G\rho_{gas}(r)}}. \quad (5)$$

We refer to $\epsilon_{\text{ff, int}}$ as the *intrinsic* star formation efficiency per free-fall time, namely, the efficiency characterizing the star formation activity of nested shells of gas, each shell being narrow enough to have its own uniform volume density $\rho(r)$ and free-fall time $\tau_{\text{ff}}(r)$. We assume that $\epsilon_{\text{ff, int}}$ is constant, varying neither as a function of radial location inside the clump, nor as a function of time.

For a pure power-law density profile of slope $-p$ $\rho_{gas}(r) \propto r^{-p}$, Eq. 4 yields (for $p < 2$):

$$SFR_{clump} = \frac{(3-p)^{3/2}}{2.6(2-p)} SFR_{TH}, \quad (6)$$

where

$$SFR_{TH} = \epsilon_{\text{ff, int}} \frac{m_{gas}}{\tau_{\text{ff}}} \quad (7)$$

is the star formation rate that the clump would have were its density profile a top-hat one (i.e. $SFR_{clump} = SFR_{TH}$ when $p = 0$). In this case, the local free-fall time $\tau_{\text{ff}}(r)$ is independent of r and equates its global counterpart $\langle \tau_{\text{ff}} \rangle$. Equation 6 is but for the numerical factor 2.6 in the denominator identical to equation 2 in Tan et al. (2006), where the numerical factor is 2.3. The difference between both stems from Tan et al. (2006) accounting for variations of $\epsilon_{\text{ff, int}}$ with the gas Mach number, while $\epsilon_{\text{ff, int}}$ is considered constant in Eq. 4.

Comparing Eq. 7 to Eq. 1, one can see that if ϵ_{ff} in Eq. 1 is the intrinsic star formation efficiency per free-fall time, Eq. 1 can only be applied to gas reservoirs of uniform density. Conversely, if Eq. 1 is applied to any star-forming region, regardless of its structure, ϵ_{ff} is necessarily the globally-measured star formation efficiency per free-fall time (Eq. 2). Equation 6 therefore provides a more reliable parameterization of the clump star formation rate as it disentangles the respective contributions of the intrinsic star formation efficiency per free-fall time and of the clump density profile. That is:

$$SFR_{clump} = \zeta \cdot SFR_{TH} = \zeta \cdot \epsilon_{\text{ff, int}} \frac{m_{gas}}{\tau_{\text{ff}}}, \quad (8)$$

where ζ is the magnification factor, namely, the factor by which the slope of the density profile of the clump enhances its star formation rate compared to the case of a top-hat profile. Comparing Eq. 8 with Eq. 2 also shows that the measured star formation efficiency per free-fall time is the product of its intrinsic counterpart and of the magnification factor ζ , that is:

$$\epsilon_{\text{ff, meas}} = \zeta \epsilon_{\text{ff, int}}. \quad (9)$$

Equation 9 thus encapsulates the degeneracy existing between the intrinsic star formation efficiency per free-fall time $\epsilon_{\text{ff, int}}$ on the one hand, and the impact ζ of the clump density profile on the other hand.

3. HINTS FROM NEARBY CLOUDS

Figure 1 shows the correlation between the number of Young Stellar Objects (YSOs) and the mass of dense gas of a sample of nearby molecular clouds studied by Kainulainen et al. (2014) (data from their table S1). It is thus akin to fig. 4 of Lada, Lombardi & Alves (2010), whose linear fit is shown by the green dashed line. We stress, however, that Lada, Lombardi & Alves (2010) and Kainulainen et al. (2014) do not define the dense gas in the same way. While Lada, Lombardi & Alves (2010) define the dense gas as gas denser than a surface density $\Sigma_{gas} = 160 M_{\odot} \cdot pc^{-2}$, Kainulainen et al. (2014) define it based on a volume/number density threshold of $\simeq 5 \cdot 10^3 cm^{-3}$. This explains why the fit from Lada, Lombardi & Alves (2010) overestimates the dense gas mass of most clouds: their (projected) dense gas mass includes foreground and background contributions with respect to what is measured by Kainulainen et al. (2014) (see also Fig. 11 in Parmentier & Pfalzner 2013). Figure 1 also depicts the steepness p of the density profile of each cloud as the symbol size, larger symbols corresponding to steeper profiles. p has been inferred from the slope of the gas density-PDF and is given as the κ parameter in table S1 of Kainulainen et al. (2014). The density profile steepness being measured over the gas density range for which the cloud is structured (i.e. the gas density-PDF is a power law; see e.g. Kritsuk, Norman, & Wagner 2011), the steepness p "covers" the dense gas (up to the spatial resolution limit; see below) but also some gas at lower volume densities.

Figure 1 shows that steeper profiles tend to top the data compared to shallower profiles. To ascertain this, we have divided the data points in two groups, located above, respectively, under, a dividing line of slope 1 whose intercept is such that there are 8 clouds in each group. Our dividing line is very similar to the linear fit of Lada, Lombardi & Alves (2010). Clouds above and below the dividing line have a mean steepness of $\langle p_{above} \rangle = 1.81 \pm 0.27$ and $\langle p_{below} \rangle = 1.51 \pm 0.14$, respectively. This suggests that the scatter of the $N_{YSO} - M_{dg}$ relation is not entirely random, and is partly driven by the gas density gradient. That is, to increase its YSO production, a cloud can either increase its dense-gas mass, or steepen the gas density profile. This is as anticipated by the model presented in Sec. 2.

When considering Fig. 1, however, one should keep in mind the following four points: (i) not all clouds are at the same evolutionary stage, and a higher YSO census may also stem from a longer star formation episode;

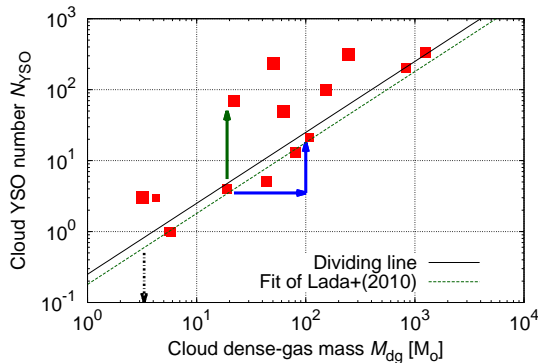


FIG. 1.— Relation between the dense gas mass and the number of YSOs of nearby molecular clouds. The downward dashed arrow indicates a starless cloud. Larger symbols code steeper gas density profiles (p is observed to range from 1.17 to 2.05; data taken from table S1 in Kainulainen et al. (2014)). The solid line is our dividing line, defined with a slope of 1 as for the fit of Lada, Lombardi & Alves (2010). It divides the cloud sample in two equal-size subsamples, with respective average values for p of $\langle p_{above} \rangle = 1.81 \pm 0.27$ and $\langle p_{below} \rangle = 1.51 \pm 0.14$. While it is commonly accepted that a cloud increases its YSO census by increasing its dense-gas mass (blue arrows), the data above suggest that it may also do so by steepening its density profile (p -increase: upward green arrow).

(ii) it is unclear which fraction of their YSOs clouds actually form in their dense gas as the existence of a gas density threshold for star formation remains debated (Parmentier 2016, 2017; Elmegreen 2018); (iii) p is unknown in the number density regime beyond the resolution limit of the observations, i.e. $> 5 \cdot 10^4 \text{ cm}^{-3}$ (Kainulainen et al. 2014); (iv) the observed YSO census measures the *past* star formation history and, therefore, results from the cloud and clump structures prevailing *before* the time t of the observations; presently-observed structures, as quantified by the observed steepness p , drive the *present and forthcoming* star formation rate. The coupling between the present-day density gradient and the past star formation rate can thus never be complete since both quantities pertain to different time-spans.

Figure 1 nevertheless constitutes a strong incentive to study the interplay between clump structure and star formation rate, especially for the uncharted regime $p > 2$, where an impact significantly stronger than for $p < 2$ is expected.

4. PRELIMINARY INSIGHTS INTO THE MODEL

We need to numerically integrate Eq. 4 to compute SFR_{clump} and to map the magnification factor

$$\zeta = \frac{SFR_{clump}}{SFR_{TH}} = \frac{\epsilon_{\text{ff, meas}}}{\epsilon_{\text{ff, int}}} \quad (10)$$

as a function of clump density profile, mass, radius and time. We assume that, at the onset of star formation (i.e. $t = 0$), the gas density profile of clumps obeys a power-law with a central core of size r_c so as to avoid a density singularity at the clump center:

$$\rho_{gas}(t = 0, r) = \frac{\rho_c}{\left[1 + \left(\frac{r}{r_c}\right)^2\right]^{p_0/2}}. \quad (11)$$

In this equation, ρ_c is the initial clump central density and $-p_0$ is the slope of the initial clump density profile when $r \gg r_c$. Both p_0 and r_c control how centrally-condensed a clump initially is and, therefore, also control its star formation rate SFR_{clump} and magnification factor ζ . All models are given an intrinsic star formation efficiency per free-fall time $\epsilon_{\text{ff, int}} = 0.01$. A model clump is thus defined by its intrinsic star formation efficiency per free-fall time, its mass m_{clump} enclosed within its radius r_{clump} (m_{clump} is equivalent to the initial gas mass), the initial steepness p_0 of its density profile and, either its initial core radius r_c , or its initial central density ρ_c , one imposing the other such that the mass enclosed within the radius r_{clump} is the clump mass m_{clump} . We run two categories of models. Firstly, we impose an initial core radius and calculate the initial gas central density ρ_c such that a mass m_{clump} is enclosed within the clump radius r_{clump} given the adopted density profile (Eq. 11). We adopt $r_c = 0.02 \text{ pc}$, which is of order the size of the circumstellar envelope of a protostar (Motte et al. 1998). The initial central density ρ_c of such models can be extremely high when they are both dense and very centrally concentrated. An example is shown in the left panel of Fig. 2. Yet, the densest known protostars have a number density $n_{H_2} \simeq 10^8 \text{ cm}^{-3}$ (Motte et al. 2018), equivalent to a mass density $\rho \simeq 7 \cdot 10^6 M_\odot \cdot \text{pc}^{-3}$. Therefore, we shall also discuss how the results for $p_0 = 3$ and $p_0 = 4$ are affected when imposing an initial central density $\rho_c = 7 \cdot 10^6 M_\odot \cdot \text{pc}^{-3}$ instead of imposing the initial core radius r_c . The panels of Fig. 2 compare the evolution with time of both types of density profiles for otherwise identical model parameters. The gas density profile at time $t > 0$ is given by eqs 18 and 19 of Parmentier & Pfalzner (2013) (equations in which $\rho_0(r)$ is the initial gas profile). We note that densities higher than $\rho_c = 7 \cdot 10^6 M_\odot \cdot \text{pc}^{-3}$ may nevertheless be relevant to specific topics, e.g. for the progenitors of the super-massive stars invoked by Denissenkov & Hartwick (2014) to explain the light-element abundance anomalies of old globular clusters.

As we shall map how the magnification factor evolves as a function of time, let us consider how the star formation rate evolves with time in this class of models. As time goes by, the mass of the gas reservoir dwindles, its volume density decreases and its free-fall time increases, all factors yielding a decreasing star formation rate (Parmentier, Pfalzner & Grebel 2014). The inner regions of a centrally-concentrated clump, due to their high density/short free-fall time, are those experiencing the fastest decrease of their gas volume density as their gas is being fed to forming stars (see Fig. 2). This is illustrated further in Fig. 3, which compares the evolution with time of a gas density profile with $p_0 = 3$ with that of a top-hat model ($p_0 = 0$) with identical mass and radius ($m_{clump} \simeq 3.2 \cdot 10^4 M_\odot$, $r_{clump} = 1 \text{ pc}$). Both models thus differ only in their initial density profile. The star formation time-span is color-coded by the right-hand-side palette. The global star formation efficiency, SFE_{gl} (i.e. the clump gas mass fraction turned into stars), achieved at any given time is significantly higher for $p_0 = 3$ than for $p_0 = 0$. As an example, Fig. 3 gives SFE_{gl} at $t = 2.5 \text{ Myr}$ for both cases. This illustrates once again that the activity of a star-forming

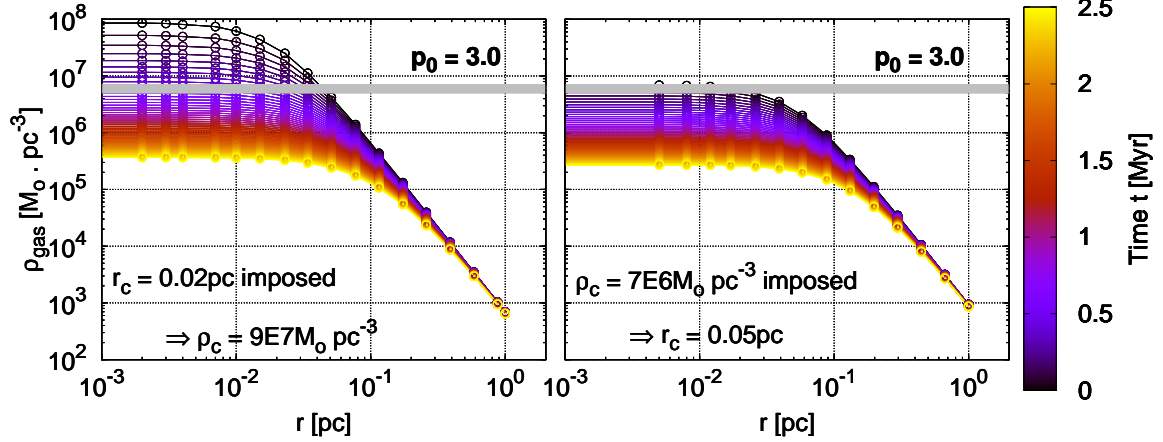


FIG. 2.— Evolution with time of the gas density profile of two model clumps. Common model parameters are $m_{clump} = 3.2 \cdot 10^4 M_{\odot}$, $r_{clump} = 1 \text{ pc}$, $p_0 = 3$ and $\epsilon_{\text{ff,int}} = 0.01$. The horizontal grey stripe depicts the density of the densest known protostars (i.e. $\rho \simeq 7 \cdot 10^6 M_{\odot} \cdot \text{pc}^{-3}$). *Left panel*: Initial core radius imposed, $r_c = 0.02 \text{ pc}$, and initial central density ρ_c inferred. *Right panel*: Initial gas central density imposed, $\rho_c = 7 \cdot 10^6 M_{\odot} \cdot \text{pc}^{-3}$, and core radius r_c inferred. The color-coding corresponds to time t after star formation onset, from 0 Myr to 2.5 Myr.

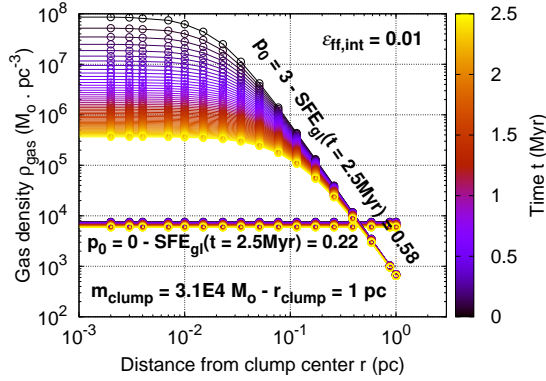


FIG. 3.— Evolution with time of the gas volume density profile of two model clumps with an intrinsic star formation efficiency per free-fall time $\epsilon_{\text{ff,int}} = 0.01$, an initial gas mass $m_{clump} \simeq 3.2 \cdot 10^4 M_{\odot}$ and a radius $r_{clump} = 1 \text{ pc}$. In one case, the gas density profile is initially a top-hat profile, and stays so through the full course of the simulations. In the other case, the parameters of the initial gas density profile are $p_0 = 3$ and $r_c = 0.02 \text{ pc}$ (see Eq. 11). The color of each profile gives the time elapsed since star formation onset (see the palette at the right-hand side).

region gets boosted simply by steepening its density profile. Since, in a centrally-concentrated clump, the inner regions are those boosting the star formation rate, once their density dwindles, the clump overall star formation rate decreases as well, with initially steeper density profiles being conducive to sharper decreases with time of the star formation rate.

This is illustrated in the top panel of Fig. 4, which presents the evolution with time of the star formation rate of 5 model clumps with the same intrinsic star formation efficiency per free-fall time, mass, radius and central core radius as in Fig. 3, but 5 different steepnesses of the density profile, from $p_0 = 0$ to $p_0 = 5$ in steps of 1. The line segments with open squares indicate the time-spans over which the global star formation efficiency SFE_{gl} has become higher than 0.5 (for $p_0 = 3$

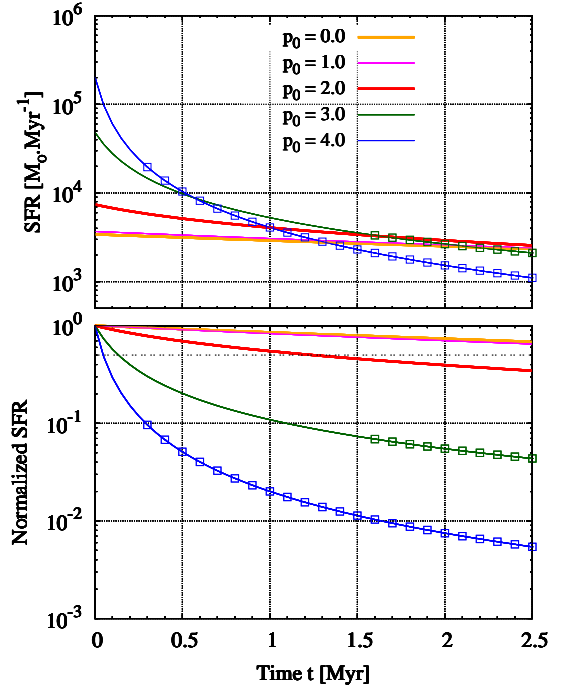


FIG. 4.— Top panel: Evolution with time of the star formation rate SFR of five model clumps, each with a different steepness p_0 of the initial gas density profile (see the key). Other parameters ($\epsilon_{\text{ff,int}}$, m_{clump} , r_{clump} and r_c) are identical to those used in Fig. 3. Bottom panel: Same as in top panel, but with the star formation rate normalized to its initial value. The black horizontal dotted line indicates when the star formation rate has dropped to half its initial value. In both panels, line segments with open squares indicate the time-spans over which the global star formation efficiency SFE_{gl} has become higher than 0.5 (which happens for $p_0 = 3$ and $p_0 = 4$ only). While the top panel highlights that a steeper gas density profile promotes a higher star formation rate initially, the bottom panel shows that it also yields a faster decline of the star formation rate with time.

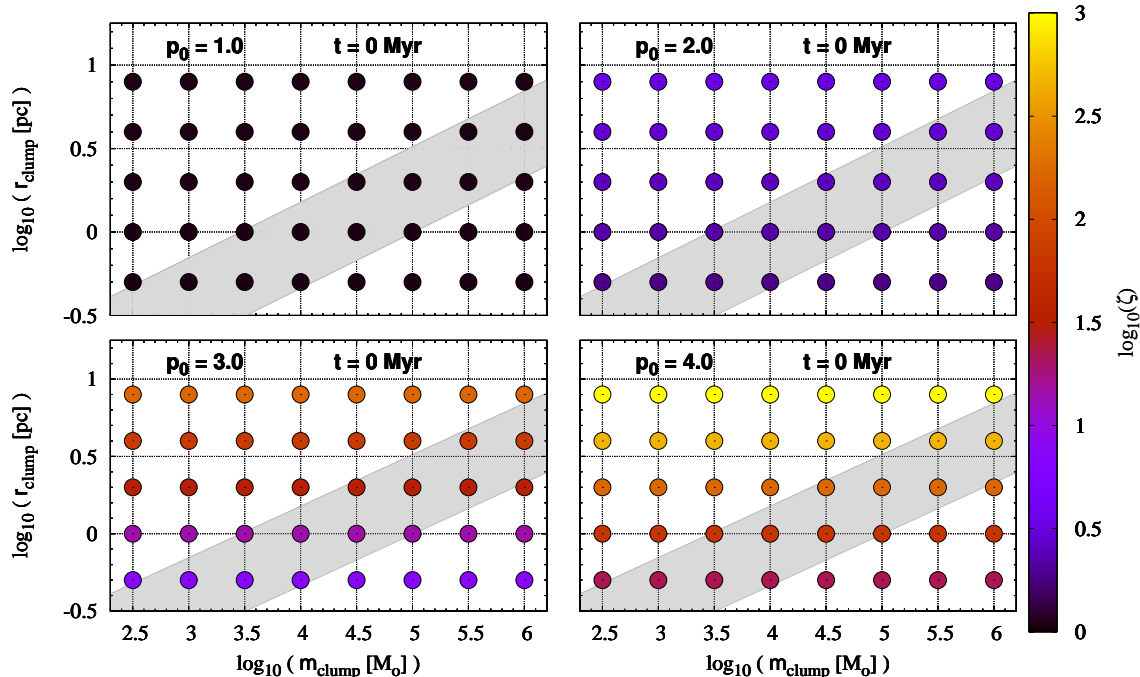


FIG. 5.— Magnification factor ζ of the star formation rate of model clumps at star formation onset (i.e. $t = 0$ Myr), with the initial core radius imposed. Parameters are the initial gas mass and radius of clumps, m_{clump} and r_{clump} , and the initial steepness p_0 of their density profile. *Top-right panel:* $p_0 = 1$. *Top-left panel:* $p_0 = 2$. *Bottom left-panel:* $p_0 = 3$. *Bottom-right:* $p_0 = 4$. The intrinsic star formation efficiency per free-fall time and the core radius of the initial gas density profile are set to $\epsilon_{ff,int} = 0.01$ and $r_c = 0.02$ pc for all simulations. Each model is represented by a plain symbol, the color of which depicts the value of ζ (see palette for color-coding, with a logarithmic scale ranging from $\zeta = 1$ to $\zeta = 10^3$). The grey stripe highlights the density regime for which steep density profiles have been detected in Galactic clouds (i.e. $10^4 \text{ cm}^{-3} < n_{H_2} < 3 \cdot 10^5 \text{ cm}^{-3} \equiv 700 M_\odot \cdot \text{pc}^{-3} < \langle \rho_{clump} \rangle < 2.1 \cdot 10^4 M_\odot \cdot \text{pc}^{-3}$; Schneider et al. 2015).

and $p_0 = 4$).

The evolution with time of the $p_0 = 0$ and $p_0 = 1$ models are very similar (compare the orange and magenta lines). Once the density profile gets steeper, however, not only does the star formation rate at star formation onset get higher, the time-scale on which the star formation rate decreases gets shorter too. This is clearly illustrated by the bottom panel of Fig. 4, which shows the star formation rate normalized to its initial value. While the model with $p_0 = 4$ loses half of its initial star formation rate in less than 0.1 Myr, the models with $p_0 = 0$ and $p_0 = 1$ need more than 2.5 Myr to do so. The star formation rate for $p_0 = 4$ decreases so fast that, in theory, it could become smaller than the star formation rate for $p_0 = 0$ (see top panel, where the blue line eventually finds itself below the orange one). For the model parameters used here and $p_0 = 4$, this is predicted to happen at $t \simeq 1.2$ Myr, when the star formation efficiency is already $SFE_{gl} = 0.77$, a case calling for gas exhaustion – rather than gas expulsion – in star-forming regions (Watkins et al. 2019).

5. MAPPING THE MAGNIFICATION FACTOR ζ

In this section, we map, and we understand, the variations of the magnification factor ζ as a function of clump parameters and time. We impose firstly an initial core radius r_c , secondly an initial central density ρ_c . The radius and mass of our model clumps extend from $r_{clump} = 0.5$ pc to 8 pc in logarithmic steps of 0.30, and from $m_{clump} = 300 M_\odot$ to $10^6 M_\odot$ in logarithmic steps

of 0.50. We remind that m_{clump} is the clump initial gas mass enclosed within r_{clump} .

5.1. r_c imposed ($r_c = 0.02$ pc) and ρ_c inferred

Results are presented in Fig. 5 for star formation onset ($t = 0$ Myr) and $r_c = 0.02$ pc. Each panel corresponds to one value of the clump profile steepness, from $p_0 = 1$ (top-left panel) to $p_0 = 2$ (top-right panel), $p_0 = 3$ (bottom-left panel) and $p_0 = 4$ (bottom-right panel). Each model clump is depicted by a plain circle whose color codes its magnification factor ζ according to the right-hand-side color palette. It should be noted that the palette gives $\log_{10}\zeta$. The maximum ζ value obtained here is $\simeq 1,300$ (for $p_0 = 4$ and $r_{clump} = 8$ pc). We caution that not the entire parameter space may be physically relevant. For instance, the top-left corner of each panel consists of clumps with a mean volume density lower than that of Galactic molecular clouds. We nevertheless include such models in the discussion so as to understand the variations of ζ through the full extent of the parameter space.

When $p_0 = 1$, clumps are barely centrally-concentrated, and their star formation rate increases by less than $\simeq 10\%$ with respect to their counterpart with $p_0 = 0$. For $p_0 = 2$, the increase becomes more noticeable, with $\zeta \simeq 2-3$.

As the profile steepness reaches $p_0 = 3$ and $p_0 = 4$, ζ truly deserves to be coined the "magnification factor". The star formation rate is indeed boosted by about two ($p_0 = 3$) and three ($p_0 = 4$) orders of magnitude

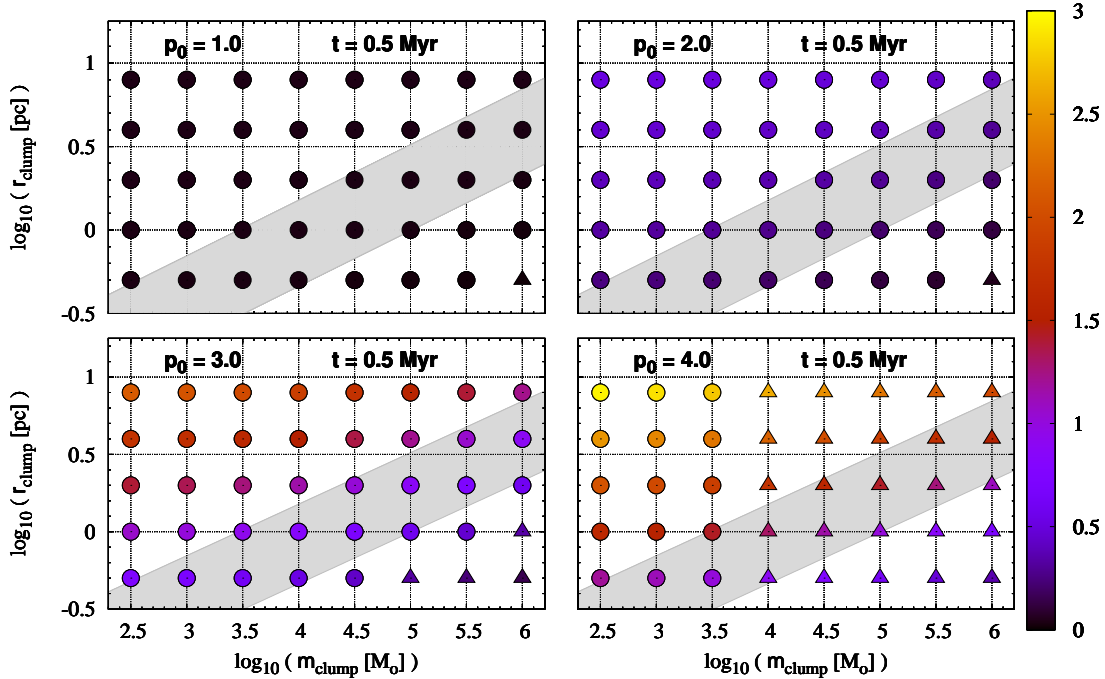


FIG. 6.— Same as in Fig. 5, but $t = 0.5$ Myr after the onset of star formation. Model clumps which by this star formation time-span have achieved $SFE_{gl} > 0.5$ are depicted by triangles

when the ratio between the core radius and the clump radius is at its smallest value (i.e. $r_c/r_{clump} = 0.0025$ when $r_{clump} = 8$ pc; top row of symbols in each panel). As for the clumps with the largest r_c/r_{clump} ratio (i.e. $r_c/r_{clump} = 0.04$ when $r_{clump} = 0.5$ pc; bottom row of symbols), the magnification factor reaches smaller, albeit still significant, values: $\zeta \simeq 7$ ($p_0 = 3$) and $\zeta \simeq 20$ ($p_0 = 4$).

For a given steepness p_0 of the initial density profile, clumps with the largest radius experience therefore the greatest star formation rate increase with respect to a homogeneous model. This is because their density profile is the most centrally-peaked, i.e. their r_c/r_{clump} ratio is the smallest (recall that r_c is kept constant). The parameterization of the clump density profile should thus not be reduced to its initial slope $-p_0$. The relative extent r_c/r_{clump} of the central core matters as well since it contributes to the central-peakedness of the clump density profile. If all models had the same r_c/r_{clump} ratio – rather than a given core radius r_c – all symbols of any given panel would have the same color. That is, the value of ζ would be independent of both m_{clump} and r_{clump} . To summarize, at $t = 0$, the magnification factor ζ depends on both p_0 and r_c/r_{clump} , i.e. $\zeta(t = 0) = \zeta(p_0, r_c/r_{clump})$.

That the measured star formation efficiency per free-fall time gets higher for smaller r_c/r_{clump} ratios is reminiscent of the results obtained by Cho & Kim (2011). For a given gas mass (i.e. the mass of their computational box), the factor by which their core formation efficiency per free-fall time is enhanced when turning-on self-gravity is higher for greater density ratios $\rho_{crit}/\langle\rho_0\rangle$, with ρ_{crit} the adopted critical density for star formation and $\langle\rho_0\rangle$ the mean volume density of the simulated gas. The

increasing factors are 2.2 and 2,400 for $\rho_{crit}/\langle\rho_0\rangle = 30$ and $\rho_{crit}/\langle\rho_0\rangle = 500$, respectively. Under the assumption of a constant critical density for star formation, this yields a higher magnification factor when the volume density of the simulated gas is lower. This is exactly as found in the semi-analytical calculations presented here since clumps of a given mass achieve greater magnification factors for lower mean volume densities (provided that r_c remains constant or varies more slowly than r_{clump}).

As explained in Sec. 4, the frantic star formation activity shown by the $p_0 = 3$ and $p_0 = 4$ models at $t \gtrsim 0$ Myr cannot be sustained for long. As the clump gas density profile loses its initial central peakedness, its star formation rate and magnification factor start to wane. Figure 6 maps the magnification factor at $t = 0.5$ Myr, showing that this one has decreased with time. Clumps having achieved a global star formation efficiency higher than 0.50 are depicted by triangles. Their ability to form stars at a fast pace results either from a high mean volume density (hence short free-fall time), or from a strongly centrally-peaked density profile (achieved either through a steep density profile, or through a smaller r_c/r_{clump} ratio), or from a combination of these factors. Note in that respect that the region of the diagram occupied by triangles is larger when $p_0 = 3$ or $p_0 = 4$ than when $p_0 = 1$ or $p_0 = 2$. Compared to Fig. 5, ζ has decreased, as is especially noticeable when $p_0 = 4$. This is so because, as we saw in the bottom panel of Fig. 4, the star formation rate decreases faster for steeper initial gas density profiles.

For each combination of p_0 and r_c/r_{clump} , that is, for each row of symbols of each panel, the decrease with time of the magnification factor is stronger for

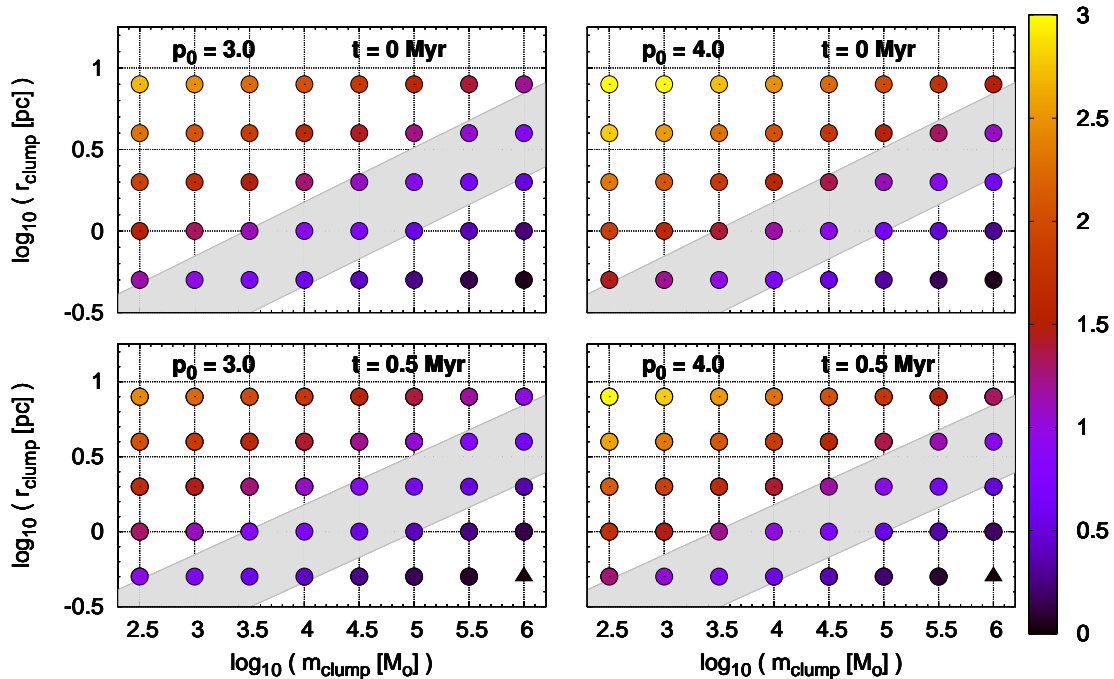


FIG. 7.— Magnification factor ζ of the star formation rate of model clumps, with the initial central density imposed. Parameters are the initial gas mass and radius of clumps, m_{clump} and r_{clump} , and the initial steepness p_0 of their density profile. *Top-left*: $p_0 = 3$ and $t = 0$ Myr. *Top-right*: $p_0 = 4$ and $t = 0$ Myr. *Bottom-left*: $p_0 = 3$ and $t = 0.5$ Myr. *Bottom-right*: $p_0 = 4$ and $t = 0.5$ Myr. The intrinsic star formation efficiency per free-fall time and the initial gas central density are set to $\epsilon_{\text{ff,int}} = 0.01$ and $\rho_c = 7 \cdot 10^6 M_\odot \cdot \text{pc}^{-3}$ for all simulations. Each model is represented by a plain symbol, the color of which depicts the value of ζ (see palette for color-coding, with a logarithmic scale ranging from $\zeta = 1$ to $\zeta = 10^3$). The grey stripe highlights the density regime for which steep density profiles have been detected in Galactic clouds (i.e. $10^4 \text{ cm}^{-3} < n_{\text{H}_2} < 3 \cdot 10^5 \text{ cm}^{-3} \equiv 700 M_\odot \cdot \text{pc}^{-3} < \langle \rho_{clump} \rangle < 2.1 \cdot 10^4 M_\odot \cdot \text{pc}^{-3}$). Model clumps which have achieved $SFE_{gl} > 0.50$ by $t = 0.5$ Myr are depicted by triangles.

more massive clumps since those have reached a more advanced stage of their evolution by virtue of their shorter mean free-fall time (see also figs 3 and 4 in Parmentier, Pfalzner & Grebel 2014). As in Fig. 5, the highest value of ζ is achieved by the largest and least massive clump (top-left corner of each panel, corresponding to $m_{clump} \simeq 300 M_\odot$ and $r_{clump} \simeq 8$ pc). For $p_0 = 3$ ($p_0 = 4$), we still find for such clumps $\zeta \simeq 130$ ($\zeta \simeq 900$) when $t = 0.5$ Myr. This stems from a high magnification factor initially, combined with a long mean free-fall time (e.g. $\langle \tau_{\text{ff}} \rangle \simeq 20$ Myr when $m_{clump} \simeq 300 M_\odot$ and $r_{clump} \simeq 8$ pc), implying that the initially high magnification factor is sustained for a longer time-span than for denser clumps.

In the density regime where steep density profiles have been detected (grey stripe), the most extreme variations of ζ are from $\simeq 20$ to $\simeq 700$ when $p_0 = 4$ and $t = 0$.

5.2. ρ_c imposed ($\rho_c = 7 \cdot 10^6 M_\odot \cdot \text{pc}^{-3}$) and r_c inferred

So far, we have imposed $r_c = 0.02$ pc and calculated the initial gas central density ρ_c so that a mass m_{clump} is enclosed within a radius r_{clump} given the adopted density profile (Eq. 11). ρ_c can thus be extremely high for models which are both dense and very centrally concentrated, such as in Fig. 3 where $\rho_c \simeq 10^8 M_\odot \cdot \text{pc}^{-3}$. Yet, the densest protostars have a number density $n_{\text{H}_2} \simeq 10^8 \text{ cm}^{-3}$, equivalent to a volume $\rho \simeq 7 \cdot 10^6 M_\odot \cdot \text{pc}^{-3}$ (table 2 in Motte et al. 2018). We now discuss how the results for $p_0 = 3$ and $p_0 = 4$ are affected when imposing a clump

initial central density $\rho_c = 7 \cdot 10^6 M_\odot \cdot \text{pc}^{-3}$ rather than a core radius $r_c = 0.02$ pc.

We first stress that this is *not* the high central density *per se* which drives the initially high magnification factor when $p_0 = 3$ and $p_0 = 4$. Should it be the case, ζ would vary with clump mass at a given clump radius in Fig. 5 since the initial central density ρ_c increases with increasing clump mass when the shape of the profile (r_c , p_0) is fixed. Rather this is the *density contrast* ρ_c/ρ_{edge} between clump centre and clump edge which drives the value of ζ (see also Elmegreen 2011). This density contrast depends on the clump radius expressed in units of the core radius and on the steepness p_0 as $\rho_c/\rho_{edge}(t=0) \simeq (r_{clump}/r_c)^{p_0}$ (see Eq. 11). These two parameters, r_{clump}/r_c and p_0 , were indeed identified in the previous section as those driving the initial magnification factor.

Results are presented in Fig. 7: $p_0 = 3$: left panels; $p_0 = 4$: right panels; $t = 0$ Myr: top panels; $t = 0.5$ Myr: bottom panels. Massive and compact clumps, to accommodate their large mass inside a given volume with a limited central density, adopt a fairly large core radius. This strongly limits their initial magnification factor in spite of the steep density profile (e.g. $r_{clump} = 1$ pc, $m_{clump} = 10^6 M_\odot$, $p_0 = 4$: $r_c = 0.28$ pc and $\zeta \simeq 2$). This is also the reason why the initial magnification factor decreases with increasing clump mass for a given clump radius and a given density profile slope (i.e. given row in a given panel): the core radius grows to accommodate the

larger gas mass, thereby smoothing the clump central-peakedness (in other words, $r_c/r_{clump} \simeq (\rho_{edge}/\rho_c)^{1/p_0}$ increases as m_{clump} increases). Despite the restriction imposed on the initial central density and therefore on the density contrast ρ_c/ρ_{edge} , clumps with $p_0 = 4$ and a mean number density in the range $10^4 < n_{H_2} < 3 \cdot 10^5 \text{ cm}^{-3}$ (i.e. the gas densities for which steep density profiles have been detected; Schneider et al. 2015) still present magnification factors ranging from $\zeta = 5$ to 25.

Based on the results shown in Figs. 5-7, we thus conclude that magnification factors up to at least $\zeta \simeq 25$ are realistic.

6. MODEL CONSEQUENCES

6.1. The measured star formation efficiency per free-fall time $\epsilon_{\text{ff,meas}}$

With the magnification factor ζ given by Eq. 10, it is clear that the degree of central concentration of a molecular clump can significantly inflate its globally-measured star formation efficiency per free-fall time $\epsilon_{\text{ff,meas}}$, thereby masking the intrinsic efficiency $\epsilon_{\text{ff,int}}$ at work in any clump region small enough to be considered of uniform density. Even if all molecular clumps had the same $\epsilon_{\text{ff,int}}$, wide variations in the measured efficiency $\epsilon_{\text{ff,meas}}$ are to be expected, reflecting clump structure variations rather than variations of the intrinsic star formation efficiency per free-fall time. $\epsilon_{\text{ff,meas}}$ is higher than $\epsilon_{\text{ff,int}}$ by the factor ζ , meaning that differences reaching an order of magnitude or more are doable. In a follow-up paper, we will show how one can estimate the intrinsic star formation efficiency per free-fall time and, from there, estimate the impact that the initial density profile of a clump has had on its past star formation rate.

6.2. Did the progenitors of old globular clusters have a steep density profile?

Rahner et al. (2019) have studied the ability of star clusters formed at the center of spherically-symmetric molecular clouds to expel the cloud gas as a function of the cloud density profile. Although the initial steepness p_0 of their models (their $-\alpha$ parameter) is not as extreme as in this paper (they range from 0 to 2), it is interesting to note that they find that steeper density profiles are less able to unbind the cloud gas. That is, the outwardly-propagating feedback-driven shell in which the cloud gas is collected is more likely to fall back onto the cluster when the density profile is steep (in their case, when $p_0 = 2$; see their fig. 4). If this gas collapse contributes a new episode of star formation in the cluster, and if this scenario repeats itself several times, it could contribute to explaining multiple stellar populations in star clusters (Rahner et al. 2018). Steep density profiles inside gaseous cluster progenitors therefore present an interesting two-fold potential: (i) they favour a high star formation efficiency (see Fig. 3) and, thus, the formation of bound clusters; (ii) they may also favour the formation of subsequent/multiple stellar populations, as those now routinely observed in Galactic old globular clusters.

7. CONCLUSIONS

Molecular clumps have a higher star formation rate when they present a volume density gradient than

when they are uniform in density (Tan et al. 2006; Girichidis et al. 2011; Cho & Kim 2011; Elmegreen 2011; Parmentier 2014). This effect arises from the clump inner regions being denser than the clump as a whole, yielding faster and more efficient star formation than would be expected based on the clump mean free-fall time (see Figs 3 and 4). In this contribution, we have expanded the model of Parmentier & Palfzner (2013) to map this effect in a systematic and comprehensive way. For this purpose, we adopt a power-law of slope $-p_0$ and central core radius r_c to describe the initial gas volume-density profile of molecular clumps (Eq. 11). We refer to p_0 as the steepness of the clump density profile. We have computed the star formation rate of clumps SFR_{clump} (Eq. 4) as a function of their mass m_{clump} , radius r_{clump} , profile steepness p_0 , and time t since star formation onset. We adopt an intrinsic star formation efficiency per free-fall time $\epsilon_{\text{ff,int}}$ to quantify the star formation activity of any clump region small enough to be considered of uniform density (see Eq. 4). This one is kept constant through all our simulations: $\epsilon_{\text{ff,int}} = 0.01$. Our models encompass 4 values of p_0 : $p_0 = 1, 2, 3, 4$, the steepest profile being observed in the high-density regions of the nearby molecular cloud NGC6334 (Schneider et al. 2015). We have run two types of model. Either we impose the central core radius ($r_c = 0.02 \text{ pc}$) and we infer the gas central density ρ_c such that a mass m_{clump} is enclosed inside the radius r_{clump} given the adopted initial density profile. Or we impose the central density ($\rho_c = 7 \cdot 10^6 M_\odot \cdot \text{pc}^{-3}$) and infer the central core radius r_c .

We refer to the ratio between the star formation rate of a centrally-concentrated clump SFR_{clump} and the star formation rate SFR_{TH} of its top-hat equivalent as the *magnification factor* ζ (Eq. 8). Gas clumps which are more centrally-concentrated – either through a smaller relative extent of the central core r_c/r_{clump} or/and through a steeper density profile – have a higher magnification factor ζ at star formation onset (see Fig. 5 and the top panels of Fig. 7). That is, their density gradient allows them to enhance their star formation rate with respect to what they would experience should they be of uniform density. As time goes by, the density profile loses part of its central peakedness (see Fig. 3) and the star formation rate decreases as a function of time, the decrease being faster for steeper density profiles (Fig. 4). As a result, the magnification factor ζ decreases with time (compare Figs 5 and 6, and the top and bottom panels of Fig. 7).

That a steep density profile amplifies the star formation rate of clumps also impacts the estimate of their star formation efficiency per free-fall time. To infer it, observers often build on the global properties of the gas reservoir under scrutiny, i.e. its mass, mean density (hence free-fall time) and star formation rate. We refer to this estimate as the *measured* star formation efficiency per free-fall time $\epsilon_{\text{ff,meas}}$ (Eq. 2). Global properties, however, do not account for the clump density profile and, therefore, renders an inflated star formation efficiency per free-fall time compared to what would be found for a uniform-density profile. The magnification factor $\zeta = SFR_{clump}/SFR_{TH}$ that we have mapped also equates the ratio between the (globally-)measured star formation efficiency per free-fall time and its *intrinsic* coun-

terpart, i.e. $\zeta = \epsilon_{\text{ff,meas}}/\epsilon_{\text{ff,int}}$ (Eq. 10). More centrally-concentrated clumps yield therefore higher measured star formation efficiencies per free-fall time. The implications are that, even for a fixed $\epsilon_{\text{ff,int}}$, its measured counterpart $\epsilon_{\text{ff,meas}}$ present wide fluctuations, reflecting the diversity of clump inner structures rather than variations in the process of star formation itself. Top-hat or shallow profiles have no or little impact on the star formation rate and, for them only, the measured star formation efficiency per free-fall time provides a sensible estimate of the intrinsic efficiency.

With this contribution we therefore encourage observers to become more cognisant of the fact that variations in their measured star formation efficiency per free-fall time are – at least partly – driven by differences in the structure of molecular clumps hosted by the star-forming regions they survey, rather than by variations in the intrinsic star formation efficiency per free-fall time itself. Our result for molecular clumps is akin to that found by

Lada, Lombardi & Alves (2010) and Lada et al. (2013) for giant molecular clouds of the Solar neighborhood, as they show that molecular clouds with a larger dense-gas fraction, e.g. more clumps, have a higher star formation rate. In this contribution we have shown that the gas distribution on the smaller spatial scale of molecular clumps matters as well.

GP is grateful to Douglas Heggie and Anna Pasquali for stimulating discussions while working on this manuscript. GP also thanks Bruce Elmegreen for having, at the Aspen meeting *Modes of Star Formation: a Symposium in Honor of Jay Gallagher*, drawn her attention to the work of Schneider et al. (2015). GP acknowledges support from the Sonderforschungsbereich SFB 881 "The Milky Way System" (subproject B5) of the German Research Foundation (DFG).

REFERENCES

- Cho, W., & Kim, J. 2011, MNRAS, 410, L8
 Denissenkov, P.A., Hartwick, F. D. A. 2014, MNRAS, 437, 21
 Elmegreen, B.G. 2011, ApJ, 731, 61
 Elmegreen, B.G. 2018, ApJ, 854, 16
 Evans, J.E. II, Dunham, M.M., Jorgensen, J.K., Enoch, M.L., Merin, B. 2009, ApJS, 181, 321
 Gao, Y; Solomon, P.M. 2004, ApJ, 606, 271
 Ginsburg, A.; Bally, J.; Barnes, A.; Bastian, N.; Battersby, C. 2018, ApJ, 853, 171
 Girichidis, P., Federrath, C., Banerjee, R., Klessen, R.S. 2011, MNRAS, 413, pp2741-2759
 Gutermuth, R.A., Pipher, J.L., Megeath, S.T., et al. 2011, ApJ, 739, 84
 Kainulainen, J., Federrath, C., Henning, Th. 2014, Science, 344, 182
 Kritsuk, A. G. and Norman, M. L. and Wagner, R. 2011, ApJ, 727, L20
 Krumholz, M.R., McKee, C.F. 2005, ApJ, 630, 250
 Krumholz, M.R., Tan, J.C. 2007, ApJ, 654, 304
 Krumholz, M.R., Dekel, A. & McKee, C.F. 2012, ApJ, 745, 69
 Lada, C.J., Lombardi, M., Alves, J.F. 2010, ApJ, 724, 687
 Lada, C.J., Lombardi, M., Roman-Zuniga, C., Forbrich, J., Alves, J.F. 2013, ApJ, 778, 133
 Motte, F., André, P., & Neri, R. 1998, A&A, 336, 150
 Motte, F., Bontemps, S., & Louvet, F. 2018, ARA&A, 56, 41
 Müller, K.E., Shirley, Y.L., Evans, N.J. II & Jacobson, H.R. 2002, ApJS, 143, 469
 Murray, N. 2011, ApJ, 729, 133
 Ochsendorf, B. B., Meixner, M., Roman-Duval, J., Rahman, M. & Evans, II, N.J. 2017, ApJ, 841, 109
 Parmentier, G., Pfalzner, S. 2013, A&A, 549, 132
 Parmentier, G. 2014, Astronomische Nachrichten, 335, 543
 Parmentier, G., Pfalzner, S. & Grebel E.K. 2014, ApJ, 791, 132
 Parmentier, G. 2016, ApJ, 826, 74
 Parmentier, G. 2017, ApJ, 843, 7
 Rahner, D., Pellegrini, E.W., Glover, S.C.O., Klessen, R.S. 2018, MNRAS, 473, L11-L15
 Rahner, D., Pellegrini, E.W., Glover, S.C.O., Klessen, R.S. 2019, MNRAS, 483, pp2547-2560
 Schneider, N., Bontemps, S., Girichidis, P., Rayner, T., Motte, F., et al 2015, MNRAS, 453, L41-L45
 Vázquez-Semadeni, E. 1994, ApJ, 423, 681
 Tan, J.C., Krumholz, M.R. & McKee, C.F. 2006, ApJ, 641, L121
 Vutisalchavakul, N.; Evans, N.J., II & Heyer, M. 2016, ApJ, 831, 73
 Watkins, E.J.; Peretto, N.; Marsch, K.; Fuller, G.A. 2019 A&A 628, 21
 Wu, J., Evans, N.J., II, Shirley, Y.L., Knez, C. 2010, ApJS, 188, 313